Giant energy transfer from an electron bunch to a photon beam mediated by radiation reaction

Probing strong-field QED in electron-photon interactions – (SQED18)

22nd August 2018

Matteo Tamburini

Alberto Benedetti   Christoph H. Keitel

Nature Photonics **12**, 319-323 (2018)

MAX-PLANCK-GESELLSCHAFT

Max Planck Institute for Nuclear Physics, Heidelberg

Why are ultrabright sources of gamma-ray beams essential?

Bright γ beams enable a broad range of new scientific and technological applications in fundamental physics, nuclear physics and laboratory astrophysics.

- Bright γ beams allow to probe the quantum vacuum and to test fundamental QED process such as the creation of matter from pure light ($\gamma\gamma \to e^- e^+$) or light-by-light scattering ($\gamma\gamma \to \gamma\gamma$), therefore providing a new route to precision tests of the Standard Model.
- Bright γ beams open the way to producing dense neutral and collimated relativistic electron–positron jets in the laboratory, and to mimic the processes that occur in astrophysical environments.
- Intense γ beams allow the first catalyzed neutral $\gamma e^- e^+$ plasma creation (QED cascade) from γ seeds instead of e^- seeds in the presence of strong laser fields. Electron seeding may be problematic (Tamburini *et al.*, Sci. Rep. **7**, 5694 (2017), Sampath *et al.*, Phys. Plasmas **25**, 083104 (2018)).
- Bright γ beams open new possibilities for high resolution nuclear spectroscopy at higher nuclear excitation energies as well as the production of large amounts of excited nuclei and isotopes or the radiography of dense objects. This may also lead to better models for the element synthesis in astrophysics.

Instability-driven magnetic field amplification

Illustration of a transverse electromagnetic instability

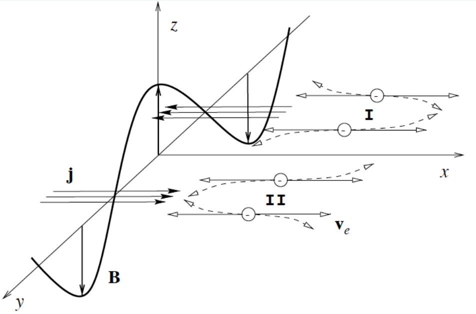

FIG. 1.—Illustration of the instability. A magnetic field perturbation deflects electron motion along the x-axis, and results in current sheets (j) of opposite signs in regions I and II, which in turn amplify the perturbation. The amplified field lies in the plane perpendicular to the original electron motion.

From Medvedev *et al.*, The Astrophysical Journal **526**, 697 (1999).

The Universe provides several examples of gamma-ray emitters: solar flares, pulsars, energetic blazars, neutron star mergers and gamma ray burst.

Gamma-ray emitters require powerful mechanisms for accelerating charged particles to relativistic energies.

These relativistic particles may propagate through a surrounding plasma and trigger the self-generation of strong magnetic fields.

The simultaneous presence of relativistic particles propagating through strong electromagnetic fields results into the copious emission of high-energy photons.

Can we reproduce similar mechanisms in the laboratory?

An instability-driven gamma-ray source, in addition to its intrinsic interest, may be a valid alternative to existing gamma-ray sources such as Compton back-scattering.

Illustration of the concept of instability-driven gamma-ray source

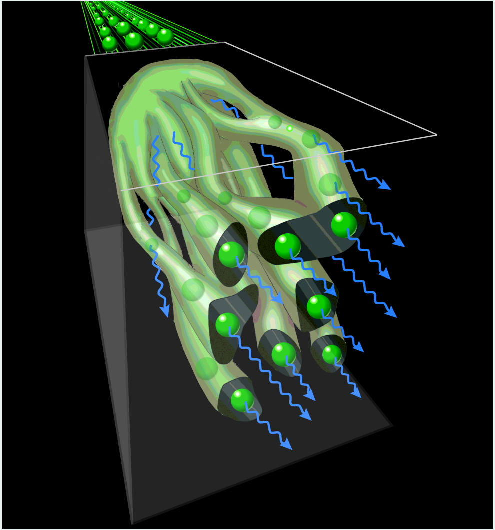

A dense ($\gtrsim 3 \times 10^{19}$ cm^{-3}) ultrarelativistic (2 GeV) electron beam with milliradiant divergence collides with a 0.5 mm thickness solid conductor.

After about 10^{-18} s the configuration of two overlapping counter-propagating currents is established and the electron beam becomes unstable to small electromagnetic fluctuations.

The development of an electromagnetic instability originates from a repulsive force between two oppositely directed currents inside the conductor. This leads to the generation of a 10^7-10^8 gauss magnetic field accompanied by a flash of gamma-rays.

Up to 60% of the electron beam energy is converted into gamma rays via synchrotron emission in strong self-generated electromagnetic fields.

Instability modes and growth rates

Many possible instability modes are simultaneously excited

In reality, when an electron beam propagates through a background plasma every possible mode allowed by Maxwell equations is triggered, with a wide range of wave vector orientations.

Filamentation and two-stream instabilities correspond to different orientation of the wave vector, i.e. transverse or longitudinal, respectively.

When an electron beam with density n_b interacts with a plasma with density n_e and plasma frequency $\omega_e = \sqrt{4\pi e^2 n_e/m_e}$, the growth rates of the instability modes are:

Two-stream instability:
$\delta_{\mathrm{TS}} \simeq \frac{\sqrt{3}}{2^{4/3}} \frac{\omega_e}{\gamma_b} \sqrt[3]{\frac{n_b}{n_e}}$

Filamentation instability:
$\delta_{\mathrm{F}} \simeq \frac{\omega_e}{\sqrt{\gamma_b}} \sqrt{\frac{n_b}{n_e}}$

Faster growing mixed two-stream-filamentation instability mode:
$\delta_{\mathrm{M}} \simeq \frac{\sqrt{3}}{2^{4/3}} \frac{\omega_e}{\sqrt[3]{\gamma_b}} \sqrt[3]{\frac{n_b}{n_e}}$

Bret *et al.*, Phys. Rev. Lett. **94**, 115002 (2005).

For an ultra-relativistic beam $\delta_{\mathrm{M}} \gg \delta_{\mathrm{F}} \gg \delta_{\mathrm{TS}}$

The mixed two-stream-filamentation instability grows faster and the electron beam is modulated both in the transverse plane and in the propagation direction.

Evolution of the transverse electron beam density

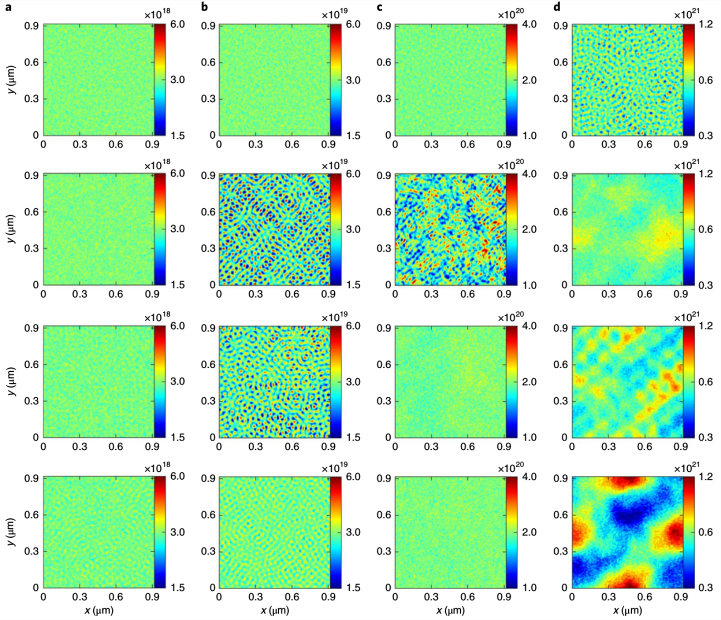

Evolution of the electron beam number density distribution in the xy plane, i.e. transverse to the beam propagation direction z.

The initial electron beam density is:
a, 3×10^{18} cm^{-3},
b, 3×10^{19} cm^{-3},
c, 2×10^{20} cm^{-3},
d, 6×10^{20} cm^{-3}.

Plots belonging to the same row report the density distribution when the beam has traveled across the same distance z inside the target. From the top to the bottom: $z = [0.2, 0.8, 2, 3] \times 10^{-2}$ cm.

Evolution of the longitudinal electron beam density

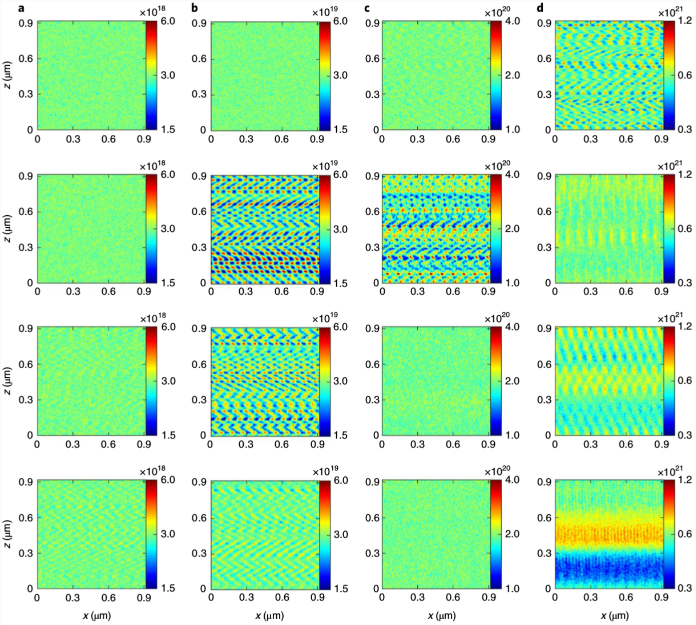

Evolution of the electron beam number density distribution in the *xz* plane, i.e. along the beam propagation direction *z*.

The initial electron beam density is: **a**, 3×10^{18} cm^{-3}, **b**, 3×10^{19} cm^{-3}, **c**, 2×10^{20} cm^{-3}, **d**, 6×10^{20} cm^{-3}.

Plots belonging to the same row report the density distribution when the beam has traveled across the same distance *z* inside the target. From the top to the bottom: $z = [0.2, 0.8, 2, 3] \times 10^{-2}$ cm.

Fields experienced by the electrons of the beam

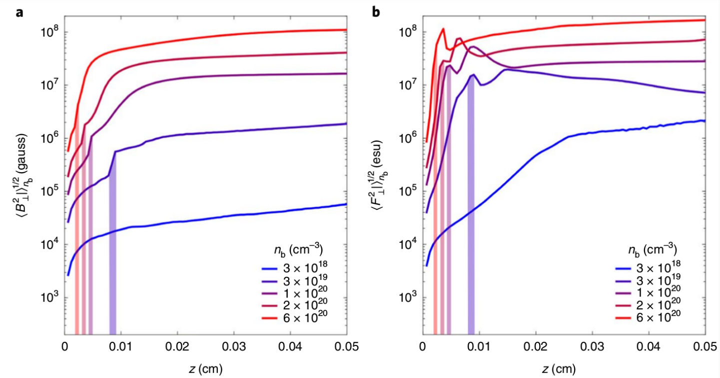

a, average transverse magnetic field experienced by the electrons of the beam $\langle B_\perp^2 \rangle_{n_b}^{1/2}$ as a function of the target thickness for different initial beam densities. **b**, same as in **a** but for the average transverse electromagnetic field experienced by the electrons of the beam $\langle F_\perp^2 \rangle_{n_b}^{1/2}$. The vertical stripes in **a** and **b** highlight the field strength amplification associated with the electromagnetic instability (only for $n_b \geq 3 \times 10^{19}$ cm^{-3}).

$$\langle B_\perp^2 \rangle_{n_b} = \left(\int d^3\boldsymbol{r}\; n_b(\boldsymbol{r}) \right)^{-1} \int d^3\boldsymbol{r}\; n_b(\boldsymbol{r}) \left[B_x(\boldsymbol{r})^2 + B_y(\boldsymbol{r})^2 \right]$$

$$\langle F_\perp^2 \rangle_{n_b} = \left(\int d^3\boldsymbol{r}\; n_b(\boldsymbol{r}) \right)^{-1} \int d^3\boldsymbol{r}\; n_b(\boldsymbol{r}) \left[\left(E_x(\boldsymbol{r}) - B_y(\boldsymbol{r}) \right)^2 + \left(E_y(\boldsymbol{r}) + B_x(\boldsymbol{r}) \right)^2 \right]$$

Gamma yield and conversion efficiency

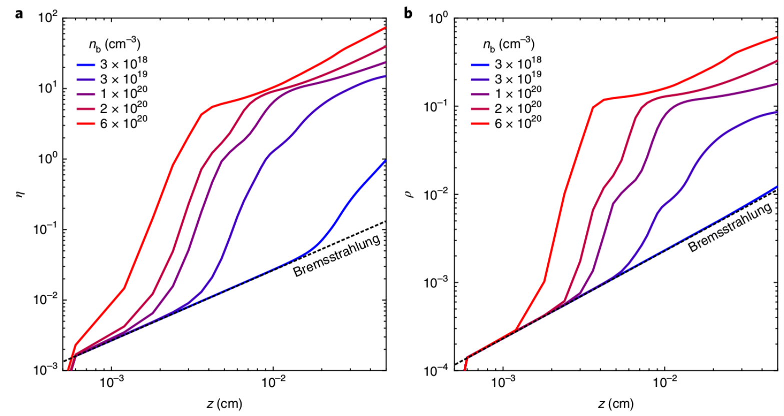

a, average number of photons emitted per electron η as a function of the target thickness for different initial beam densities. **b**, the same as in **a** for the electron-to-photon energy conversion efficiency ρ, defined as the ratio between the photon and the initial beam total energies. In both panels the black dashed line shows the expected value for a pure bremsstrahlung emission.

A. Benedetti, M. Tamburini, C. H. Keitel, Nature Photonics **12**, 319-323 (2018).

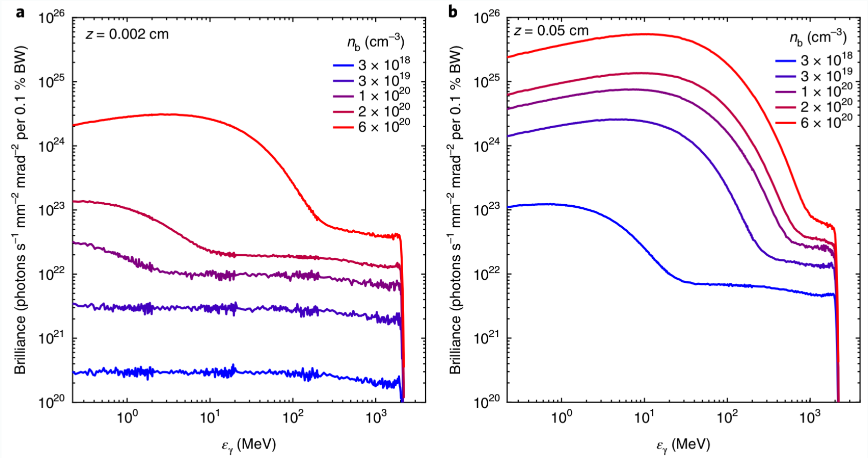

The gamma-ray brilliance as a function of the emitted photon energy ϵ_γ and as a function of the initial electron beam density n_b.

a, after the electron beam has traversed $z = 0.002$ cm, and

b, after the electron beam has traversed $z = 0.05$ cm within the target.

A. Benedetti, M. Tamburini, C. H. Keitel, Nature Photonics **12**, 319-323 (2018).

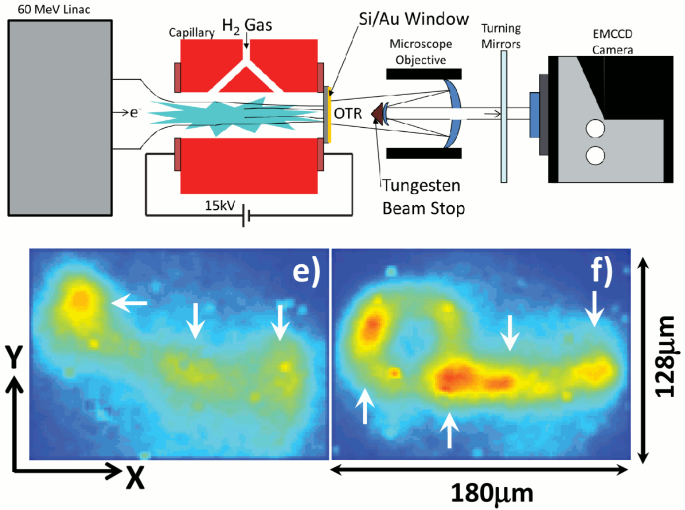

Images of the bunch at the capillary exit with arrows indicating filaments. Electron beam parameters $\sigma_{0x} \sim 80$ μm $\sigma_{0y} \sim 50$ μm and 1 nC charge corresponding to a beam density of 1.9×10^{17} cm^{-3}. Much lower electron and plasma density and much colder beam than in our case ($\Delta_{p_x} = \Delta_{p_y} = 3.6$ MeV$/c$ and $\Delta_{p_z} = 144$ MeV$/c$ initial momentum distributions).

B. Allen, V. Yakimenko, M. Babzien, M. Fedurin, K. Kusche, P. Muggli, Phys. Rev. Lett. **109**, 185007 (2012).

eli delivery consortium

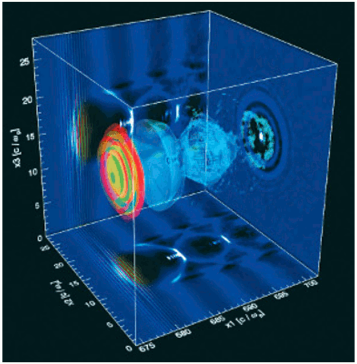

FACET

FACET-II Beam Parameters

Beam energy (GeV)	10
Repetition Rate (Hz) **(range)**	10 1-30
Bunch Charge (nC) **(range)**	2 0.5-3
Bunch Length (σ, μm) **(range)**	20 1-100
Beam Spot size (σ, μm) **(range)**	10 5-200

Electron beams with density of the order of 3 x 10^{19} cm^{-3} and energy above 1 GeV with 10 Hz repetition rate will allow to obtain unprecedented gamma-ray sources.

Summary & Conclusions

An electron-beam-instability-driven gamma-ray source

We have put forward a new concept of laboratory gamma-ray source, which reproduces mechanisms similar to those of astrophysical environments. The electromagnetic instability associated with a dense, ultrarelativistic electron beam colliding with a 0.5 millimeter thickness conductor results into strong self-generated fields (10^7-10^8 gauss) accompanied by an ultrabright collimated gamma-ray flash. The major features are:

- A relatively simple setup is required. In contrast to Compton backscattering, there are no issues with beam alignment and synchronization.
- The energy of gamma-ray photons range from approximately 100 keV to several GeV and beyond.
- In principle, this gamma-ray source can operate at kHz repetition rate.
- Unprecedented conversion efficiency. Up to 60% of the electron beam energy can be converted into an ultrabright gamma-ray flash.
- A plethora of applications are possible. A bright gamma-ray source may open up the production of electron–positron plasmas from pure light in the laboratory, and allows the investigation of nonlinear quantum electrodynamics phenomena such as light-by-light scattering, offering a complementary route to experiments with large particle colliders.

Cross sections

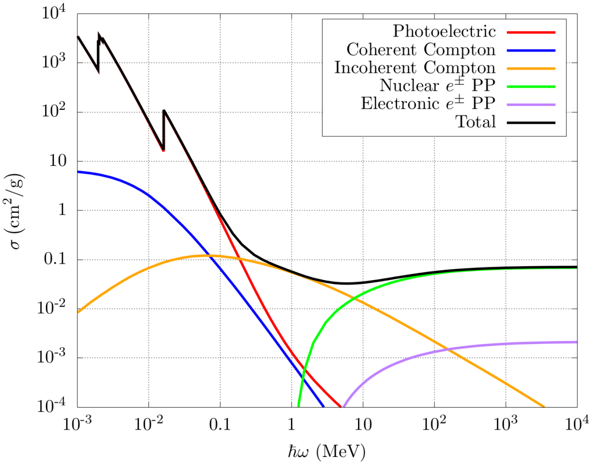

Photon cross sections as a function of the photon energy in Strontium (Z = 38) showing the contributions from the atomic photoelectric effect (electron ejection, photon absorption), coherent (Rayleigh scattering, atom neither ionised nor excited) and incoherent Compton scattering as well as pair production in the nuclear and in the electron fields, respectively.

A. Benedetti, M. Tamburini, C. H. Keitel, Nature Photonics **12**, 319-323 (2018).

Intensity attenuation

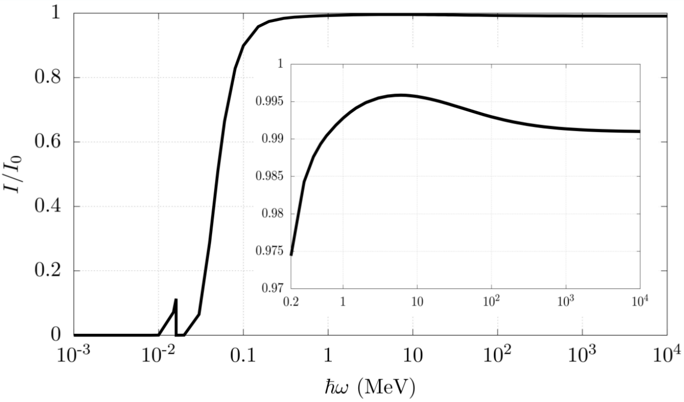

Fraction of the photon beam intensity I/I_0 emerging from a metallic Strontium ($Z = 38$) target with thickness $z_{\max} = 0.05$ cm and density $d = 2.54$ g/cm^3 as a function of the photon energy. The inset displays a zoom of the plot in the range $I/I_0 \in [0.97, 1]$ and $\hbar\omega \in [0.2$ MeV, 10 GeV$]$.

A. Benedetti, M. Tamburini, C. H. Keitel, Nature Photonics **12**, 319-323 (2018).

Breit-Wheeler pair production

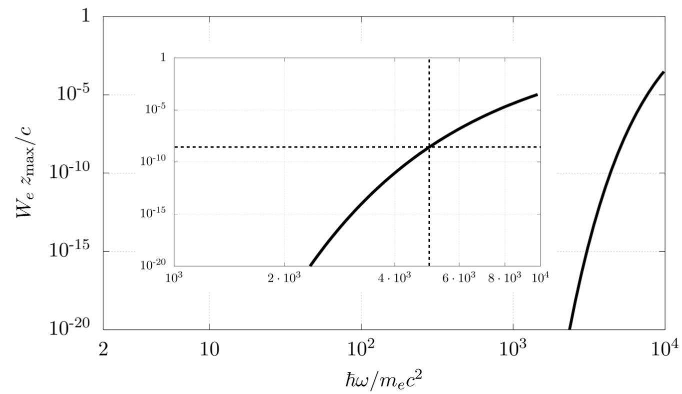

Probability for a single photon with energy $\hbar\omega$ to produce an electron-positron pair when it travels a distance $z_{\max} = 0.05$ cm in the presence of a constant electromagnetic field $F_\perp = 10^9$ esu. The inset displays a zoom of the plot in the range $\hbar\omega \in [10^3, 10^4] m_e c^2$. The vertical dashed line corresponds to the maximum photon energy considered in our work $\hbar\omega_{\max} = 2.5$ GeV and the horizontal dashed line highlights the corresponding electron-positron pair production probability of about 10^{-8}.

A. Benedetti, M. Tamburini, C. H. Keitel, Nature Photonics **12**, 319-323 (2018).

Collisional and collisionless simulation results for $n_b = 3 \times 10^{19} cm^{-3}$.

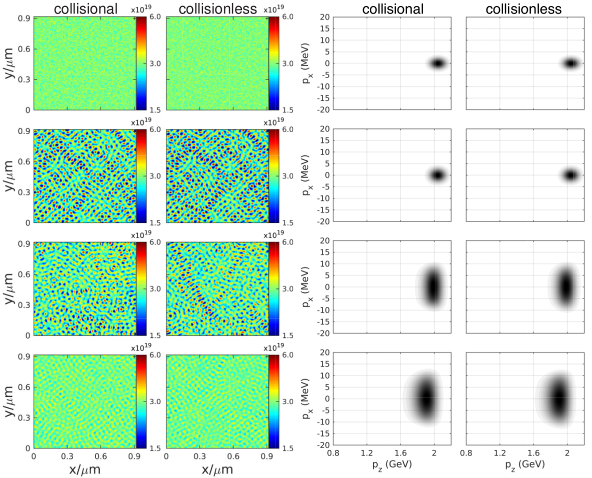

a, Evolution of the electron beam number density distribution in the plane perpendicular to the beam propagation direction with (left column) and without (right column) collisions. **b**, evolution electron beam momentum distribution in the *pzpx*-plane, the electron beam propagating along the z-axis, with (left column) and without (right column) collisions. The plots belonging to the same row report the results obtained when the beam has travelled across the same distance z inside the target. From the top to the bottom: $z = [0.2, 0.8, 2, 3] \times 10^{-2}$ cm.

The transverse electromagnetic field

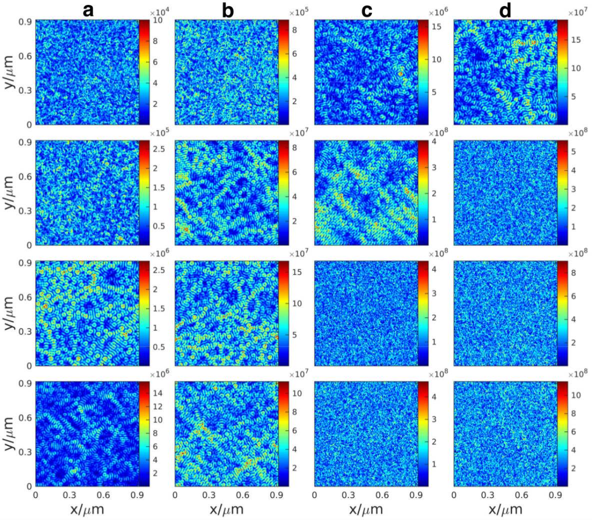

Evolution of the transverse electromagnetic field $F_\perp$ in the plane perpendicular to the beam propagation direction, which is along the z-axis. The initial electron beam density is: **a**, $n_b = 3 \times 10^{18}$ cm^{-3}, **b**, 3×10^{19} cm^{-3}, **c**, 2×10^{20} cm^{-3}, **d**, 6×10^{20} cm^{-3}. Snapshots belonging to the same row are taken at the same distance z inside the target. Note the quite different scale of each snapshot due to the large variations of $F_\perp$. From the top to the bottom: $z = [0.2, 0.8, 2, 3] \times 10^{-2}$ cm.

Local-constant-field approximation

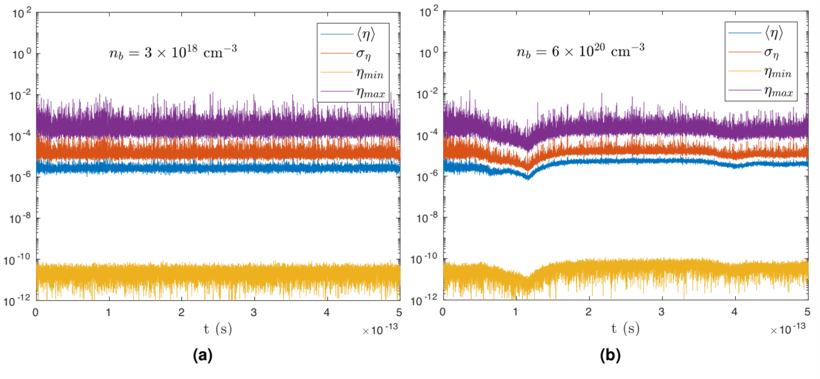

Evolution of the parameter $\eta = |\dot{F}|\Delta\tau/F$, which provides an estimate of the validity of the LCFA. Here $\langle\eta\rangle$, σ_η, $eta_{textmin}$ and $eta_{textmax}$ are the average, standard deviation, minimum and maximum value of η obtained from a sample of 1024 electrons of the beam initially uniformly distributed in the whole 3D computational box.

A. Benedetti, M. Tamburini, C. H. Keitel, Nature Photonics **12**, 319-323 (2018).

The transverse electron beam momentum

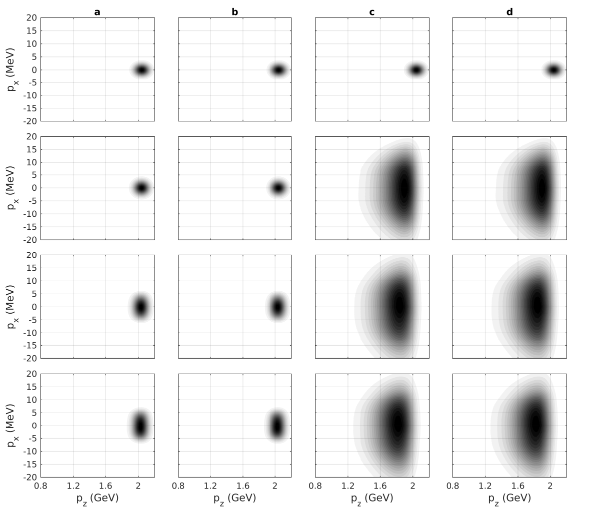

Evolution of the distribution of the transverse electron beam momentum, i.e. in the plane $p_x p_y$ orthogonal to the beam propagation direction. Snapshots belonging to the same row are taken at the same distance z inside the target. From the top to the bottom: $z = [0.2, 0.8, 2, 3] \times 10^{-2}$ cm.

A. Benedetti, M. Tamburini, C. H. Keitel, Nature Photonics **12**, 319-323 (2018).